ACS NANO
Cite This: ACS Nano 2018, 12, 4903–4908
www.acsnano.org

ARTICLE

Ultrathin Piezotronic Transistors with 2 nm Channel Lengths

Longfei Wang,[†,‡,▲] Shuhai Liu,[§,▲] Guoyun Gao,[†,‡] Yaokun Pang,[†,‡] Xin Yin,[⊥] Xiaolong Feng,[#] Laipan Zhu,[†,‡] Yu Bai,[†,‡] Libo Chen,[†,‡] Tianxiao Xiao,[†,‡] Xudong Wang,[⊥] Yong Qin,*[,§,∥] and Zhong Lin Wang*[,†,‡,¶]

[†]CAS Center for Excellence in Nanoscience, Beijing Key Laboratory of Micro-nano Energy and Sensor, Beijing Institute of Nanoenergy and Nanosystems, Chinese Academy of Sciences, Beijing 100083, China
[‡]College of Nanoscience and Technology, University of Chinese Academy of Sciences, Beijing 100049, China
[§]School of Advanced Materials and Nanotechnology, Xidian University, Xi'an, 710071, China
[∥]Institute of Nanoscience and Nanotechnology, School of Physical Science and Technology, Lanzhou University, Lanzhou 730000, China
[⊥]Department of Materials Science and Engineering, University of Wisconsin—Madison Madison, Wisconsin 53706, United States
[#]Microsystems and Terahertz Research Center, China Academy of Engineering Physics, Chengdu, Sichuan 610200, China
[¶]School of Material Science and Engineering, Georgia Institute of Technology, Atlanta, Georgia 30332, United States

Supporting Information

ABSTRACT: **Because silicon transistors are rapidly approaching their scaling limit due to short-channel effects, alternative technologies are urgently needed for next-generation electronics. Here, we demonstrate ultrathin ZnO piezotronic transistors with a ∼2 nm channel length using inner-crystal self-generated out-of-plane piezopotential as the gate voltage to control the carrier transport. This design removes the need for external gate electrodes that are challenging at nanometer scale. These ultrathin devices exhibit a strong piezotronic effect and excellent pressure-switching characteristics. By directly converting mechanical drives into electrical control signals, ultrathin piezotronic devices could be used as active nanodevices to construct the next generation of electromechanical devices for human−machine interfacing, energy harvesting, and self-powered nanosystems.**

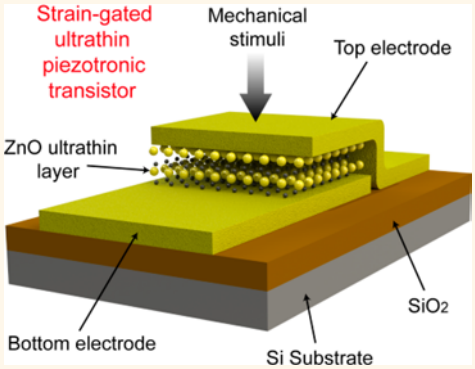

KEYWORDS: *piezotronic transistor, ZnO ultrathin film, piezotronics, piezoelectricity, piezotronic effect*

Fabrication of sub-5 nm silicon (Si) transistors is extremely challenging due to the weakening effectiveness of electrostatic gate control on the channel.[1] Transistors based on carbon nanotubes,[2−4] nanowires,[5] and two-dimensional transition metal dichalcogenides[6,7] have been explored for breaking through the size limit, but the operation of these devices still relies on the mechanism of external voltage gating.[2−7] Piezotronic transistors using inner-crystal piezopotential as the gate voltage have been demonstrated for wurtzite structured semiconductors.[8−11] Such devices are innovative in a way that the traditional channel width gating is replaced by interface gating, with a possibility of breaking through the channel width to sub-nanometer scale. However, the currently reported piezotronic transistors were made of nanowires that had sizes on the order of a few micrometers. Thus, it is unknown if such devices can be shrunk to sub-nanometer scale, although they are gated by interface polarization charges distributed within one to two atomic layers at the metal−semiconductor interface.

Piezoelectricity in bulk crystals, films, and nanowires has wide applications in transducers, energy harvesting, and electronics.[12−16] A rapid development of high-performance and miniaturized electronic devices in nano-electromechanical systems (NEMS)[16,17] calls for synthesis and discovery of low-dimensional piezoelectric materials. Many transition metal dichalcogenides (TMDs) are proposed theoretically as outstanding two-dimensional (2D) in-plane piezoelectric materials.[18,19] Monolayer MoS_2-based powering nanodevices and piezoelectric sensors have demonstrated possible applications of 2D nanomaterials in nanoscale electromechanical devi-

Received: March 15, 2018
Accepted: April 27, 2018
Published: April 27, 2018

DOI: 10.1021/acsnano.8b01957
ACS Nano 2018, 12, 4903−4908

ces.[20−24] However, the anisotropy of in-plane piezoelectricity and the great challenge to achieve large-scale directional growth of TMD monocrystals seriously impede actual integration into devices.[6,20−24] Recently, sub-nanometer-thick platelets with wurtzite structure (Figure 1a), such as ZnO[25] and CdS[26] with

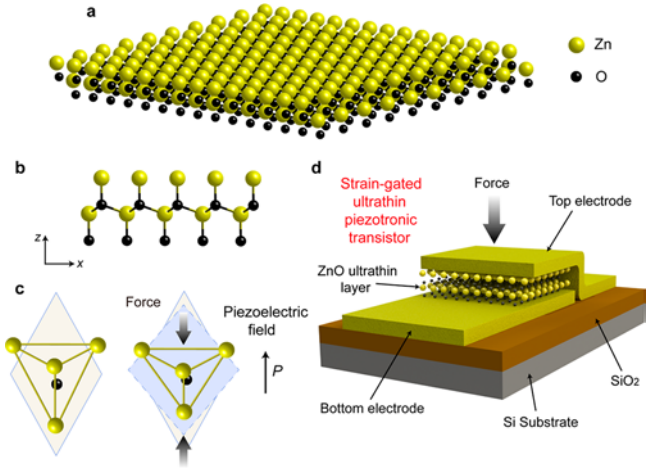

Figure 1. Strong out-of-plane piezoelectricity in ultrathin ZnO material with wurtzite structure for ultrathin piezotronic transistors. (a) Ultrathin ZnO materials with wurtzite structure. (b) View of the ZnO structure from the side. (c) ZnO nanomaterials with a hexagonal structure consisting of Zn−O−Zn stacking, with the O atom centered in the tetrahedron (left). A piezoelectric field points along the *c*-axis when the unit cell of ZnO nanomaterial is compressed by external force in the *z*-direction (right). (d) Schematic illustration of an ultrathin piezotronic transistor with two-terminal configuration. The stress-induced strong out-of-plane piezopotential in ZnO ultrathin film can effectively modulate the metal−semiconductor barriers to control the carrier transport.

polarization direction normal to the nanosheets, have been synthesized. The hexagonal structure of ZnO is still preserved even when its thickness is as low as a few atomic layers, so that the crystal with noncentrosymmetry structure still has piezoelectric properties. Simply, metal cation Zn and anion O are tetrahedrally coordinated, and their centers overlap with each other (Figure 1b,c, left). By applying stress along an apex of the tetrahedron, the centers of positive and negative ions are displaced relatively, resulting in a piezoelectric polarization (Figure 1c, right), which is the origin of the piezoelectricity along the *c*-axis, which is usually the normal direction of the grown nanosheets of ZnO.

Here, using the piezoelectric polarization charges presented on the surfaces within one to two atomic layer thickness, ultrathin piezotronic transistors were demonstrated with a physical channel length of ∼2 nm, as shown in Figure 1d. The stress-induced strong out-of-plane piezopotential can effectively modulate charge carrier transport. This study shows the effectiveness of the "gating" effect of the piezopotential within an ultrashort channel length in the 2D wurtzite structures, with potential applications for energy harvesting, ultrasensitive sensors, and nanoscale electromechanical systems.

RESULTS AND DISCUSSION

The single-crystalline ZnO ultrathin films were prepared at the water−air interface.[25] In the synthesis process, oleylsulfate monolayer was used as a template to guide the growth of ZnO nanostructures, resulting in ZnO ultrathin films at the water−air interface with the *c*-axis perpendicular to the liquid level pointing to air (Figure S1). A typical morphology of the as-obtained ZnO ultrathin films is a single triangular with edges from ∼10 to 40 μm (Figure S2) and a thickness of ∼2 nm (Figure 2a). Transmission electron microscopy (TEM) and

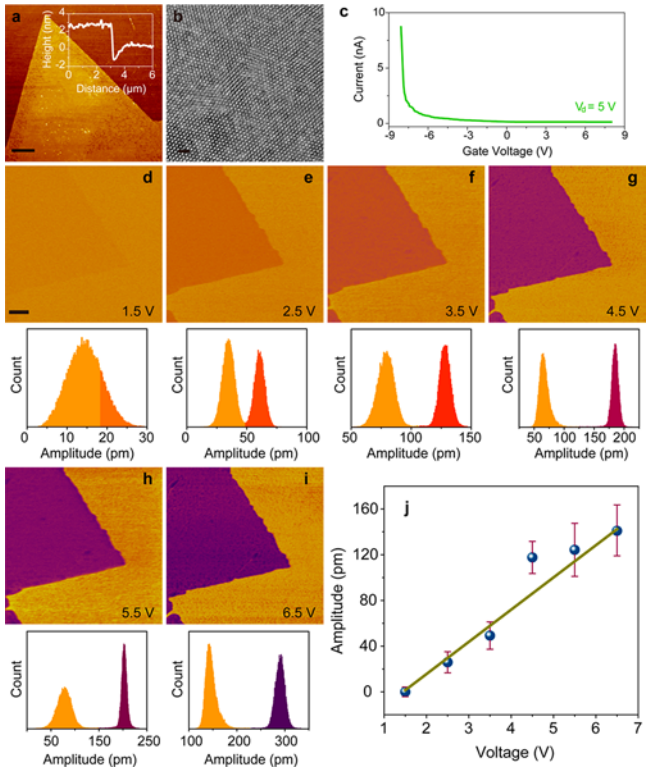

Figure 2. Materials characterization. (a) Atomic force microscopy topography scans of typical ultrathin film. Scale bar, 3 μm. (b) HRTEM image of the ZnO ultrathin film. Scale bar, 1 nm. (c) Electronic property of ZnO ultrathin film demonstrates that the ZnO ultrathin film is p-type. (d−i) Amplitudes *versus* applied voltages (1.5−6.5 V) showing inverse piezoelectricity. The insets are statistical distribution of amplitude values of ZnO ultrathin film and substrate. Scale bars, 500 nm. (j) Average amplitude variations *versus* applied voltages derived from the statistical distributions of amplitude values of ZnO ultrathin film and substrate (d−i). Error bars indicate standard deviations. The piezoelectric coefficient d_{eff} is evaluated to be ∼23.7 pm·V^{-1}.

high-resolution TEM (HRTEM) images reveal the single-crystal structure of the ultrathin film (Figure S3 and Figure 2b). In the water−air growth method, an oleylsulfate monolayer was inevitably adsorbed on the ZnO ultrathin films. X-ray photoelectron spectroscopy (XPS) was used to confirm the presence of oleylsulfate on the surface of the ZnO ultrathin film (Figure S4). With a thickness of only a few nanometers, the molecules of oleylsulfate might have a great impact on the electrical property of ZnO ultrathin film.[27,28] The simulated structure of wurtzite ZnO ultrathin film and corresponding electronic band structures show that the ZnO ultrathin film is a direct band gap p-type semiconductor.[25] The electronic property of ZnO ultrathin film was further investigated by fabricating field-effect transistors (FETs). The I_d−V_g curve presents a typical p-type semiconductor behavior (Figure 2c). Moreover, this atom thick p-type semiconductor can be stable

DOI: 10.1021/acsnano.8b01957
ACS Nano 2018, 12, 4903−4908

in the atmospheric environment, making it an ideal choice for constructing ultrathin electronic devices.

For ultrathin piezoelectric devices, the piezoelectricity is the key factor that directly determines the mechanism and performance. Here, we used piezoresponse force microscopy[29,30] (PFM) to investigate the out-of-plane piezoelectricity of ZnO ultrathin film (Figure S5). Conductive PFM was applied to characterize the vertical piezoresponse of ZnO ultrathin film with the tip's voltages from 1.5 to 6.5 V. The amplitude images and corresponding topography and phase images under different tip voltages are presented in Figure 2d–i and Figure S6. As expected, obvious amplitude changes were found as the tip voltage increased continuously, indicating a strong inverse piezoelectric effect. The insets are statistical distributions of amplitude values of the ZnO and the substrate. The overall amplitude changes of ZnO *versus* applied voltages can be derived from entire areas from Figure 2d–i, and the calculation method is detailed in Figure S7. By deriving the slope of the amplitudes *versus* the voltages, the effective piezoelectric coefficient (d_{eff}) of ZnO ultrathin film is calculated to be ~23.7 pm·V^{-1} (Figure 2j). It is about two times larger than that of the bulk ZnO materials and even larger than that of some inorganic ferroelectric ceramics (Table S1). The strong out-of-plane piezoelectricity of ZnO ultrathin film makes it an ideal candidate for ultrathin piezoelectric devices. According to previous studies, the piezoelectricity strongly depends on the carrier concentration of materials.[31] For example, as the carrier concentration changed from 10^9 to 10^{18} cm^{-3}, the piezoelectric coefficient of CdS will be decreased by 60%.[32] Based on the dimension of the ZnO ultrathin film and the conductance, the carrier concentration was estimated to be ~10^{12} cm^{-2}.[25] Therefore, this strong out-of-plane piezoelectricity of ZnO ultrathin film is presumably due to the low carrier concentration and the changes in local polarization.

We next measured the electrical transport property of ultrathin piezotronic transistors under compressive stress at room temperature. The two-terminal devices fabricated with metal–semiconductor–metal structure (Figure 3a) consist of two Schottky barriers. Its conductance is dominated by the reversed metal–ZnO Schottky contact (Figure 3c and Figure S8). The changed electrical transport behavior probably resulted from two effects. One is the piezotronic effect,[9,20,33−37] 37 in which stress-induced piezoelectric polarization charges at metal–semiconductor interfaces asymmetrically modulate the Schottky barriers. The other is the piezoresistive effect, in which stress-induced band gap or charge carrier density change modulate the entire resistance of the device, resulting in a symmetric volume effect without polarity. For the ultrathin piezotronic transistor, under compressive stresses, the current significantly increases under forward bias and gradually decreases under reverse bias (Figure 3b). This asymmetric modulation indicates that the modulation of charge carrier transport is dominated by the piezotronic effect. According to the Schottky theory, a linear relationship between ln(I) and $V^{1/4}$ or V corresponds to the presence or absence of the mirror force at the Schottky junction. By plotting both ln(I)–$V^{1/4}$ and ln(I)–V curves, we found that the ln(I) is almost proportional to $V^{1/4}$ (Figure S9), indicating that there exists a mirror force at the Schottky junction, and the barrier is not that "sharp". In addition, the changes of Schottky barrier height calculated in Figure S10 shows an approximately linear relationship with applied pressures, further demonstrating that the stress-induced piezopotential can effectively modulate the Schottky barrier. By

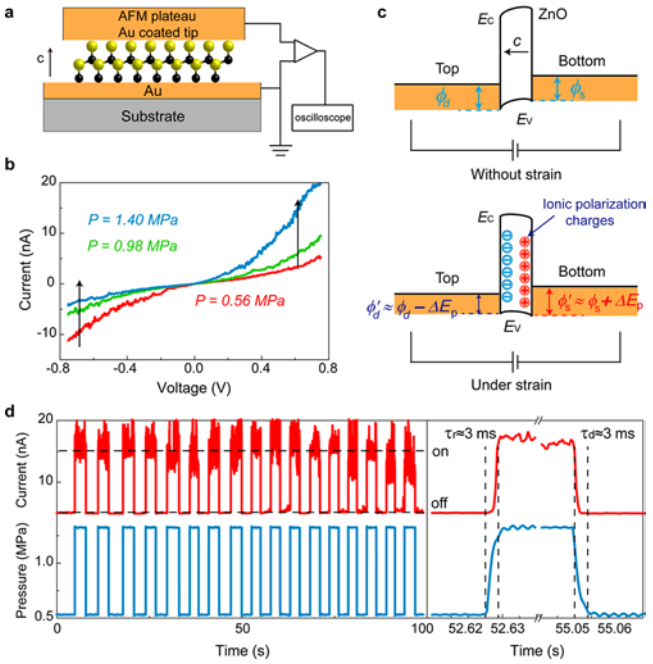

Figure 3. Electrical transport properties of ultrathin piezotronic transistor with metal–semiconductor–metal structure under stress. (a) Cross-sectional view of the structure of an ultrathin piezotronic transistor together with atomic force microscopy measurement used to characterize the device. (b) Asymmetric modulation of carrier transport by stress in ultrathin piezotronic transistor shows characteristics of piezotronic effect. (c) Band diagrams explaining that the piezotronic behavior occurred in ultrathin piezotronic transistor. φ_d and φ_s represent the Schottky barrier heights formed at contacts. ΔE_p indicates the change of Schottky barrier height by piezoelectric polarization charges. (d) Real-time measurement of the current through an ultrathin piezotronic transistor that reversibly switches between the closed and open forms upon pressure pulses at a bias of 1.0 V (left). The current responses are between 52 and 56 s (right).

deriving the ln(dI/dV)–V curves from the nonlinear fitting of I–V characterization (Figure S11), we do not find any singularity or discontinuity which would occur in a tunneling case, indicating that there is almost no tunneling current in the ultrathin ZnO piezotronic transistor.

Upon applying the compressive stress, a strong piezoelectric field can be produced inside the ZnO ultrathin film because of the strong out-of-plane piezoelectricity (Figure 2j) and atomic thickness of ZnO (~2 nm, Figure 2a), which has a profound influence not only on the carriers' concentration and distribution in ZnO ultrathin film but also on the charge distribution in metal–semiconductor interface states.[10,33−37] Generally, the negative piezopotential can attract holes from the interface, resulting in a decreased barrier height, whereas the positive piezopotential can deplete holes toward the interface, resulting in an increased barrier height (Figure 3c).[8−12,33−37] The polarity of stress-induced piezoelectric polarization charges cause an opposite modulation on the barrier height of the metal–semiconductor contacts, as well as the anisotropic changes in electrical transport of ultrathin piezotronic transistors. The magnitude and polarity of the piezopotential depend on the crystallographic orientation of the piezoelectric semiconductor and direction of stress. Consequently, the carrier transport across the metal–semiconductor contacts can be effectively modulated by the

DOI: 10.1021/acsnano.8b01957
ACS Nano 2018, 12, 4903–4908

piezoelectric polarization charges, which can be controlled by the external stress. Hence, the mechanical stress can function as a controlling gate signal, and no external gate voltage is required for a piezotronic transistor. The controllable regulation in ultrathin devices by stress-induced out-of-plane piezopotential may offer an approach for tunable electronics.

To investigate the responsiveness of ultrathin piezotronic transistors to the applied mechanical stimuli, we measured the current's response to periodically switched stresses at a constant bias of 1.0 V (Figure 3d (left) and Figure S12). The dynamic response indicates that the impact of compressive stress on the conductance is reversible. The measured current is immediately increased as the compressive stress increased and immediately restored to its original state as the compressive stress is removed, which can be considered as "on/off" states in a transistor and may enable the development of next-generation logic circuits. The response is highly repeatable in many on/off cycles, and no obvious degradation is observed, indicating a good repeatability and stability. The current responds very quickly to the change of stress, and the response time of the ultrathin piezotronic transistor is about ~3 ms (Figure 3d, right), which can also be enhanced by integrating local on-site signal processing circuits[38] with an ultrathin piezotronic transistor.

Next, piezotronic stress-gated OR logic gates were developed using a series of ultrathin piezotronic transistors (Figure 4 and Figure S13). The forces were independently applied on the respective components of the piezotronic stress-gated logic gates. Four states, "00", "01", "10", and "11", defined here correspond to four combinations of off (0) and on (1) for the two equal and independently controlled forces. The measured currents for the "00" state were only ~2 nA under a bias of 2.0 V; in contrast, the measured currents were ~7 nA for the "01" and "10" states (Figure 4b,d). The charge carrier transport of an ultrathin piezotronic transistor is dominated by the reversed Schottky barrier, which is formed between top electrodes and ultrathin film. Under a single compressive force (Figure 4a,c), negative piezopotential induced on the top Schottky contact decreases the barrier height and hence increases the electrical transport of the device (Figure 4b,d), as schematically illustrated by the band diagrams (Figure 3c). In the "11" state, with both forces applied simultaneously, the measured current was significantly enhanced and much larger than that of "01" and "10" states (Figure 4e,f). In this case, both the reverse-biased Schottky barriers were decreased by the negative piezopotential generated by ZnO ultrathin films. Taken all together, the stress-gated series of ultrathin piezotronic transistors demonstrated the spatially resolved various logic gates controlled by mechanical force, which may have applications in electronic skin, human–machine interfacing, and nanorobotics. These results demonstrate that the piezotronic effect is still effective at ultrathin junctions, although further efforts are still required to achieve large-scale fabrication of ultrathin piezotronic transistors for practical applications.

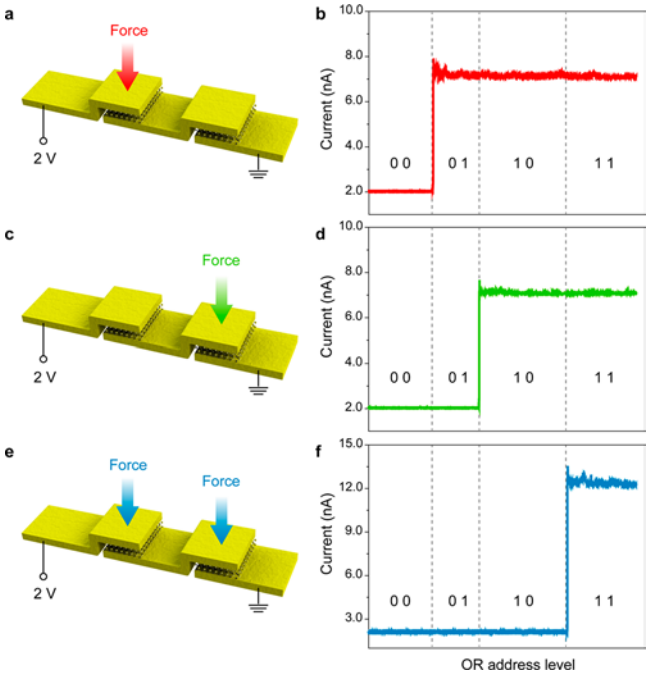

Figure 4. Stress-gated OR logic gates using a series of ultrathin piezotronic transistors. (a,b) OR gate with one force on and the measured output currents for the "01" state. (c,d) OR gate with one force on and the measured output currents for the "10" state. (e,f) OR gate with the both forces on and the measured output currents for the "11" state. The current is much smaller in the "00" state than in the "01", "10", and "11" states. The current is much larger in the "11" state than in "01" and "10" states.

CONCLUSIONS

In summary, we have successfully developed ultrathin ZnO piezotronic transistors with a ~2 nm physical channel length. The charge carrier transport characteristics of our devices can be effectively gated by the piezoelectric polarization charges created at the metal–semiconductor interface. The atomic thickness of ZnO and the structure of a two-terminal piezotronic transistor enable the study of their physics at ultrashort channel by using the strong out-of-plane piezoelectricity, removing the need for an external gate electrode or any other patterning processes that are challenging at these scale lengths. This work provides insight into the development of high-performance transistors with ultrashort channels, as an alternative to conventional silicon technologies. This study also proves the potential application of ultrathin piezoelectric materials in next-generation electronics.

METHODS

Synthesis of ZnO Ultrathin Films. We synthesized ZnO ultrathin films by using a water–air method. In a typical preparation of ZnO ultrathin films, 25 mM $Zn(NO_3)_2$ and hexamethylenetetramine were added into 17 mL of aqueous solution. Then, 10 μL of chloroform solution containing 0.1 vol % sodium oleyl sulfate was spread on the aqueous solution surface. Then, this solution was placed in a 60 °C convection oven. A single layer of ZnO ultrathin films appeared in about 100 min.

ZnO Ultrathin Film Morphology and Band Structure Characterization. For atomic force microscopy (AFM), scanning electron microscopy, and XPS characterization, ZnO ultrathin films were transferred to SiO_2/Si substrates. The morphology and thickness of the ZnO ultrathin films were characterized by using AFM tapping mode (MFP-3D, Asylum Research) and a HITACHI S-8020 field-emission scanning electron microscope. The force constant of Si tips is 2.8 N/m, and the resonance frequency is ~75 kHz. TEM analysis was performed by using a FEI TECNAI F20 microscope. XPS was performed on an ESCALAB 250 instrument from Thermo Fisher Scientific, USA.

Fabrication of the FET Device and Electrical Measurement. The ZnO ultrathin films were transferred onto the Si wafer with 300 nm thermally grown SiO_2. The devices were fabricated by standard e-

DOI: 10.1021/acsnano.8b01957
ACS Nano 2018, 12, 4903–4908

beam lithography (EBL) process as follow: First, a layer of 200 nm positive e-beam photoresist (MICRO CHEM 950 PMMA A4) was spin-coated on the substrate at 4000 rpm for 60 s and then baked at 150 °C for 5 min. Then, the source/drain electrodes were subsequently defined by standard EBL, electron-beam evaporation of Cr/Au (10 nm/40 nm), and a lift-off process. The electrical characterization of the devices was conducted with a semiconductor parameter analyzer (Agilent B1500A) in a probe station under ambient environment.

Piezoresponse Force Microscopy Imaging To Investigate the Out-of-Plane Piezoelectricity of ZnO Ultrathin Film. The out-of-plane piezoelectricity of ZnO ultrathin films was performed using AFM (MFP-3D, Asylum Research) with PFM mode. The conductive tips of Pt/Ir coating, with the force constant of 2.8 N/m, were used in PFM mode. The resonance frequency is ~380 kHz for PFM mode. In order to accurately calculate the deformation of ZnO ultrathin film under different voltages, we count the amplitude values of ZnO and the substrate from entire areas. Then, the average amplitude variations of ZnO *versus* applied voltages can be calculated by subtracting the amplitude values of the substrate. To form weak indentation, a force of ~150 nN was applied to the sample surface. All samples were examined in a sealed chamber under ambient laboratory conditions.

Fabrication of Single Ultrathin Piezotronic Transistor and Electrical Measurement. Cr/Au (10 nm/50 nm) was deposited on the prepared substrates as the bottom electrode through RF magnetron sputtering. Then, the ZnO ultrathin films were transferred onto the substrate with the bottom electrode. The Au-coated AFM plateau tips (with diameter of ~1.8 μm and spring constant of ~48.31 nN/nm) were used as the top electrodes of an ultrathin piezotronic transistor to form a metal−semiconductor−metal structure. The electrical transport properties of ultrathin piezotronic transistors under compressive stress were characterized by conductive AFM measurement mode.

Fabrication of Ultrathin Piezotronic Transistors and Electrical Measurement. The devices were fabricated by standard EBL process as follow: First, a layer of 200 nm positive e-beam photoresist (MICRO CHEM 950 PMMA A4) was spin-coated on the substrate at 4000 rpm for 60 s and then baked at 150 °C for 5 min. Then, the source/drain electrodes were subsequently defined by standard EBL, electron-beam evaporation of Cr/Au (10 nm/40 nm) as the bottom electrode, and lift-off process. Then, the ZnO ultrathin films were transferred onto the bottom electrodes. Finally, the top Cr/Au electrodes were prepared by the standard EBL process. The $I-V$ characteristics of the devices were measured by a measurement system with a low-noise current preamplifier (model no. SR570, Stanford 329 Research Systems, Inc.) and a function generator (model no. DS345, Stanford Research Systems, Inc.). The forces were applied to the piezotronic transistors by using the AFM system (MFP-3DTM, Asylum Research). The measurements were taken at room temperature of ~25 °C, and the humidity was ~15%.

ASSOCIATED CONTENT

Supporting Information

The Supporting Information is available free of charge on the ACS Publications website at DOI: 10.1021/acsnano.8b01957.

Materials and methods, Figures S1−S13, and Table S1 (PDF)

AUTHOR INFORMATION

Corresponding Authors

*E-mail: qinyong@xidian.edu.cn.

*E-mail: zhong.wang@mse.gatech.edu.

ORCID

Xin Yin: 0000-0002-4759-0226

Xudong Wang: 0000-0002-9762-6792

Yong Qin: 0000-0002-6713-480X

Zhong Lin Wang: 0000-0002-5530-0380

Author Contributions

▲L.W. and S.L. contributed equally to this work.

Notes

The authors declare no competing financial interest.

ACKNOWLEDGMENTS

We thank to Fei Wang for stimulating discussions. This research was supported by the "thousands talents" program for pioneer researcher and his innovation team, China, National Natural Science Foundation of China (Grant Nos. 51322203, 51472111, 51432005, 5151101243, and 51561145021), the National Key R&D Project from Minister of Science and Technology (2016YFA0202704), and the National Program for Support of Top-notch Young Professionals.

REFERENCES

(1) Franklin, A. D. Nanomaterials in Transistors: From High-Performance to Thin-Film Applications. *Science* **2015**, *349*, aab2750.

(2) Shulaker, M. M.; Hills, G.; Patil, N.; Wei, H.; Chen, H.; Wong, H.-S. P.; Mitra, S. Carbon Nanotube Computer. *Nature* **2013**, *501*, 526−530.

(3) Cao, Q.; Tersoff, J.; Farmer, D. B.; Zhu, Y.; Han, S. J. Carbon Nanotube Transistors Scaled to a 40-Nanometer Footprint. *Science* **2017**, *356*, 1369−1372.

(4) Qiu, C.; Zhang, Z.; Xiao, M.; Yang, Y.; Zhong, D.; Peng, L. M. Scaling Carbon Nanotube Complementary Transistors to 5-nm Gate Lengths. *Science* **2017**, *355*, 271−276.

(5) Duan, X. F.; Niu, C. M.; Sahi, V.; Chen, J.; Parce, J. W.; Empedocles, S.; Goldman, J. L. High-Performance Thin-Film Transistors Using Semiconductor Nanowires and Nanoribbons. *Nature* **2003**, *425*, 274−278.

(6) Zhao, M. V.; Ye, Y.; Han, Y. M.; Xia, Y.; Zhu, H. Y.; Wang, S. Q.; Wang, Y.; Muller, D. A.; Zhang, X. Large-Scale Chemical Assembly of Atomically Thin Transistors and Circuits. *Nat. Nanotechnol.* **2016**, *11*, 954−959.

(7) Desai, S. B.; Madhvapathy, S. R.; Sachid, A. B.; Llinas, J. P.; Wang, Q.; Ahn, G. H.; Pitner, G.; Kim, M. J.; Bokor, J.; Hu, C.; Wong, H. S. P.; Javey, A. MoS_2 Transistors with 1-Nanometer Gate Lengths. *Science* **2016**, *354*, 99−102.

(8) Wang, Z. L. Nanopiezotronics. *Adv. Mater.* **2007**, *19*, 889−892.

(9) Wu, W.; Wen, X.; Wang, Z. L. Taxel-Addressable Matrix of Vertical-Nanowire Piezotronic Transistors for Active and Adaptive Tactile Imaging. *Science* **2013**, *340*, 952−957.

(10) Wu, W.; Wei, Y.; Wang, Z. L. Strain-Gated Piezotronic Logic Nanodevices. *Adv. Mater.* **2010**, *22*, 4711−4715.

(11) Han, W.; Zhou, Y.; Zhang, Y.; Chen, C.; Lin, L.; Wang, X.; Wang, S.; Wang, Z. L. Strain-Gated Piezotronic Transistors Based on Vertical Zinc Oxide Nanowires. *ACS Nano* **2012**, *6*, 3760−3766.

(12) Zhang, Y.; Yan, X.; Yang, Y.; Huang, Y.; Liao, Q.; Qi, J. Scanning Probe Study on the Piezotronic Effect in ZnO Nanomaterials and Nanodevices. *Adv. Mater.* **2012**, *24*, 4647−4655.

(13) Qin, Y.; Wang, X.; Wang, Z. L. Microfibre-Nanowire Hybrid Structure for Energy Scavenging. *Nature* **2008**, *451*, 809−813.

(14) Kingon, A. I.; Srinivasan, S. Lead Zirconate Titanate Thin Films Directly on Copper Electrodes for Ferroelectric, Dielectric and Piezoelectric Applications. *Nat. Mater.* **2005**, *4*, 233−237.

(15) Ferren, R. A. *Advances in Polymeric Piezoelectric Transducers*; Nature Publishing Group, 1991; Vol. *350*, pp 26−27.

(16) Wang, Z. L.; Song, J. H. Piezoelectric Nanogenerators Based on Zinc Oxide Nanowire Arrays. *Science* **2006**, *312*, 242−246.

(17) Nguyen, T. D.; Deshmukh, N.; Nagarah, J. M.; Kramer, T.; Purohit, P. K.; Berry, M. J.; McAlpine, M. C. Piezoelectric Nanoribbons for Monitoring Cellular Deformations. *Nat. Nanotechnol.* **2012**, *7*, 587−593.

DOI: 10.1021/acsnano.8b01957
ACS Nano 2018, 12, 4903−4908

(18) Michel, K. H.; Verberck, B. Theory of Elastic and Piezoelectric Effects in Two-Dimensional Hexagonal Boron Nitride. *Phys. Rev. B: Condens. Matter Mater. Phys.* **2009**, *80*, 224301.
(19) Duerloo, K. A. N.; Ong, M. T.; Reed, E. J. Intrinsic Piezoelectricity in Two-Dimensional Materials. *J. Phys. Chem. Lett.* **2012**, *3*, 2871−2876.
(20) Wu, W. Z.; Wang, L.; Li, Y. L.; Zhang, F.; Lin, L.; Niu, S. M.; Chenet, D.; Zhang, X.; Hao, Y. F.; Heinz, T. F.; Hone, J.; Wang, Z. L. Piezoelectricity of Single-Atomic-Layer MoS_2 for Energy Conversion and Piezotronics. *Nature* **2014**, *514*, 470−474.
(21) Qi, J.; Lan, Y. W.; Stieg, A. Z.; Chen, J. H.; Zhong, Y. L.; Li, L. J.; Chen, C. D.; Zhang, Y.; Wang, K. L. Piezoelectric Effect in Chemical Vapour Deposition-Grown Atomic-Monolayer Triangular Molybdenum Disulfide Piezotronics. *Nat. Commun.* **2015**, *6*, 7430.
(22) Wu, W.; Wang, L.; Yu, R.; Liu, Y.; Wei, S. H.; Hone, J.; Wang, Z. L. Piezophototronic Effect in Single-Atomic-Layer MoS_2 for Strain-Gated Flexible Optoelectronics. *Adv. Mater.* **2016**, *28*, 8463−8468.
(23) Zhang, X.; Liao, Q.; Liu, S.; Kang, Z.; Zhang, Z.; Du, J.; Li, F.; Zhang, S.; Xiao, J.; Liu, B.; Ou, Y.; Liu, X.; Gu, L.; Zhang, Y. Poly(4-styrenesulfonate)-induced sulfur vacancy self-healing strategy for monolayer MoS_2 homojunction photodiode. *Nat. Commun.* **2017**, *8*, 15881.
(24) Zhu, H. Y.; Wang, Y.; Xiao, J.; Liu, M.; Xiong, S. M.; Wong, Z. J.; Ye, Z. L.; Ye, Y.; Yin, X. B.; Zhang, X. Observation of Piezoelectricity in Free-Standing Monolayer MoS_2. *Nat. Nanotechnol.* **2015**, *10*, 151−155.
(25) Wang, F.; Seo, J. H.; Luo, G. F.; Starr, M. B.; Li, Z. D.; Geng, D. L.; Yin, X.; Wang, S. Y.; Fraser, D. G.; Morgan, D.; Ma, Z. Q.; Wang, X. D. Nanometre-Thick Single-Crystalline Nanosheets Grown at The Water-Air Interface. *Nat. Commun.* **2016**, *7*, 10444.
(26) Wang, X.; He, X.; Zhu, H.; Sun, Li.; Fu, W.; Wang, X.; Hoong, L. C.; Wang, H.; Zeng, Q.; Zhao, W.; Wei, J.; Jin, Z.; Shen, Z.; Liu, J.; Zhang, T.; Liu, Z. Subatomic Deformation Driven by Vertical Piezoelectricity From CdS Ultrathin Films. *Sci. Adv.* **2016**, *2*, e1600209−e1600209.
(27) Wagner, S. R.; Zhang, P. P. Surfaces and Interfaces of Nanoscale Silicon Materials. *MRS Online Proc. Libr.* **2013**, *1550*, 609−620.
(28) Zhao, P. D.; Kiriya, D.; Azcatl, A.; Zhang, C. X.; Tosun, M.; Liu, Y. S.; Hettick, M.; Kang, J. S.; McDonnell, S.; KC, S.; Guo, J. H.; Cho, K.; Wallace, R. M.; Javey, A. Air Stable P-doping of WSe_2 by Covalent Functionalization. *ACS Nano* **2014**, *8*, 10808−10814.
(29) Kalinin, S. V.; Bonnell, D. A. Imaging Mechanism of Piezoresponse Force Microscopy of Ferroelectric Surfaces. *Phys. Rev. B: Condens. Matter Mater. Phys.* **2002**, *65*, 125408.
(30) Johann, F.; Hoffmann, A.; Soergel, E. Impact of Electrostatic Forces in Contact-Mode Scanning Force Microscopy. *Phys. Rev. B: Condens. Matter Mater. Phys.* **2010**, *81*, 094109.
(31) Scrymgeour, D. A.; Hsu, J. W. P. Correlated Piezoelectric and Electrical Properties in Individual ZnO Nanorods. *Nano Lett.* **2008**, *8*, 2204−2209.
(32) Ogawa, T.; Oikawa, H.; Kojima, A. Decrement Caused by Screening Effect of Conduction Electrons on The Effective Charge of CdS Crystals. *J. Appl. Phys.* **1971**, *10*, 593−599.
(33) Zhang, Z.; Liao, Q.; Yu, Y.; Wang, X.; Zhang, Y. Enhanced Photoresponse of ZnO Nanorods-based Self-Powered Photodetector by Piezotronic Interface Engineering. *Nano Energy* **2014**, *9*, 237−244.
(34) Zhang, Y.; Yang, Y.; Gu, Y.; Yan, X.; Liao, Q.; Li, P.; Zhang, Z.; Wang, Z. Performance and Service Behavior in 1-D Nanostructured Energy Conversion Devices. *Nano Energy* **2015**, *14*, 30−48.
(35) Wang, Z. L. Piezopotential Gated Nanowire Devices: Piezotronics and Piezo-Phototronics. *Nano Today* **2010**, *5*, 540−552.
(36) Wang, Z. L.; Wu, W. Piezotronics and Piezo-Phototronics: Fundamentals and Applications. *Natl. Sci. Rev.* **2014**, *1*, 62−90.
(37) Wu, W.; Wang, Z. L. Piezotronics and Piezo-phototronics for Adaptive electronics and Optoelectronics. *Nat. Rev. Mater.* **2016**, *1*, 16031.
(38) Nemeth, B.; Symes, M. D.; Boulay, A. G.; Busche, C.; Cooper, G. J. T.; Cumming, D. R. S.; Cronin, L. Real-Time Ion-Flux Imaging in The Growth of Micrometer-Scale Structures and Membranes. *Adv. Mater.* **2012**, *24*, 1238−1242.

DOI: 10.1021/acsnano.8b01957
ACS Nano 2018, 12, 4903−4908